Ostwald Ripening in Nanoalloys: When Thermodynamics Drives a Size-Dependent Particle Composition

D. Alloyeau,[1,*] G. Prévot,[2] Y. Le Bouar,[3] T. Oikawa,[4] C. Langlois,[1] A. Loiseau,[3] and C. Ricolleau[1]

[1]*Laboratoire Matériaux et Phénomènes Quantiques, Université Paris 7/CNRS, UMR 7162, Bâtiment Condorcet, 4 rue Elsa Morante, 75205 Paris Cedex 13, France*

[2]*Institut des Nanosciences de Paris, Université Paris 6/CNRS, UMR 7588, 140 rue de Lourmel 75015 Paris, France*

[3]*Laboratoire d'Etude des Microstructures, ONERA/CNRS, B.P. 72, 92322 Châtillon, France*

[4]*JEOL Ltd, 1-2 Musashino 3-Chome, Akishima, Tokyo 196-8558, Japan*

(Received 1 September 2010; published 16 December 2010)

Ostwald ripening has been broadly studied because it plays a determinant role in the evolution of cluster size during both chemical and physical synthesis of nanoparticles. This thermoactivated process causes large particles to grow, drawing material from the smaller particles, which shrink. However, this phenomenon becomes more complex when considering the coarsening of metallic alloy clusters. The present experimental and theoretical investigations show that the relative composition of CoPt nanoparticles can be strongly modified during high temperature annealing and displays a size-dependent behavior. This compositional change originates from the higher evaporation rate of Co atoms from the nanoparticles. More importantly, this effect is expected in all alloy clusters containing species with different mobilities.

DOI: 10.1103/PhysRevLett.105.255901 PACS numbers: 65.80.−g, 68.35.bd, 68.37.Lp, 68.43.Jk

Metallic alloy clusters, also called nanoalloys, are attracting increasing attention because of the immense technological potential that arises from the combination of size effects with composition effects. However, the design of nanosystems with new and tunable properties requires understanding the phenomena that influence cluster size and composition. Ostwald ripening, first described by the Lifshitz-Slyozov-Wagner theory [1,2], is a major mechanism in the heat-induced size change of nanoparticles (NPs) on a substrate [3] or in solution [4]. If NPs' coarsening has been intensively studied, very little attention has been paid to the impact of this phenomenon on the composition of nanoalloys [5,6]. Here, energy dispersive x-ray (EDX) nanoanalysis carried out on a transmission electron microscope provides evidence that the relative composition of CoPt NPs can be strongly modified during annealing and displays a size-dependent behavior. This effect, explained within a thermodynamical framework, is expected in all nanoalloys containing species with different mobilities.

NP thin films were produced by pulsed laser deposition [7–9]. This method allows the fabrication of NP thin films with a strict control over the targeted composition ($\pm$ 2 at. %) [7]. Commercial TEM Cu grids on which a 10-nm-thick amorphous carbon film was deposited were used as the substrate. Following the synthesis, the specimens were covered with a 2-nm-thick layer of amorphous Al_2O_3 deposited by pulsed laser deposition to protect the NPs from air oxidation. Two samples with a nominal thickness of 1 nm were prepared at room temperature (as-grown NPs, sample *A*) and were subsequently annealed for 1 h at 650 °C (sample *B*) and 750 °C (sample *C*), respectively. Reference samples with the same nominal thickness of pure Pt and pure Co NPs were also grown and annealed for 1 h at 700 °C.

TEM experiments were carried out on a JEM-2100F field-emission electron microscope operating at 200 kV and equipped with a JED 2300T EDX analyzer from JEOL. To calibrate the x-ray analyzer, we determined the Cliff-Lorimer *k* factor [10] with a $Co_{45}Pt_{55}$ reference bulk sample [11]. We performed single particle composition measurements by using a 1 nm-size scanning probe [12]. Depending on the size of the NPs, the absolute error on the composition of a single sub-10 nm NP was estimated to lie between 3% and 5%, when considering the statistical fluctuations associated with the integrated counts below the Pt M and Co K peaks at a 95% confidence level [13].

Very generally, NPs' size and shape evolve during annealing as a consequence of Ostwald ripening and coalescence. The morphology of CoPt nanoparticles before and after annealing procedures is shown in Fig. 1. The mean size and polydispersity (that is, standard deviation divided

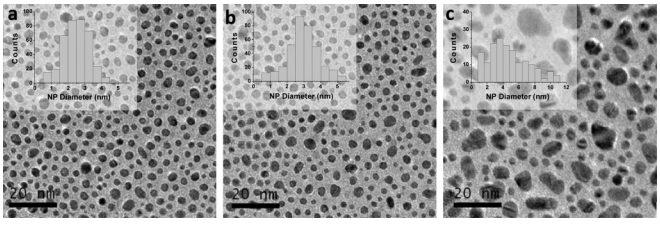

FIG. 1. TEM images of CoPt NPs with the corresponding particle size distribution in the insets. (a) As-grown NPs (sample *A*), (b) NPs after 1 h at 650 °C (sample *B*), and (c) NPs after 1 h at 750 °C (sample *C*).

by the mean size) of as-grown NPs are 3 nm and 33%, respectively [sample *A*, Fig. 1(a)]. As previously reported [7,14], growth mechanisms are weakly active below 700 °C in CoPt NPs embedded in an amorphous matrix. Consequently, the size and polydispersity of the NPs remain unchanged after 1 h at 650 °C [sample *B*, Fig. 1(b)], whereas we observe a substantial increase of the NPs' size and polydispersity (4.8 nm and 45%, respectively) after 1 h at 750 °C [sample *C*, Fig. 1(c)].

Standard EDX measurements, performed in a TEM on NP assemblies of samples *A*, *B*, and *C*, indicate a composition close to the equiatomic stoichiometry (± 1 at. %). We then undertook EDX nanoanalysis for simultaneously analyzing size and composition of single NPs. As observed in Fig. 2, the composition of the particles in samples *A* and *B* is found to be $Co_{50}Pt_{50}$ with a dispersion of ±5%, which is very close to the absolute error on the composition measurements of single sub-10 nm clusters. Moreover, the composition of the particles does not show any dependence with their size. However, in sample *C*, EDX nanoanalyses reveal a clear correlation between particle size and composition: the Co-to-Pt ratio increases with the particle size. Indeed, the largest particles in a size range from 6 to 10 nm formed by the growth mechanisms during annealing present a large excess of cobalt (68 ± 4 at. %), whereas particles below 3 nm present a lower cobalt concentration (45 ± 5 at. %). Unfortunately, it was not possible to measure the composition of very small particles (less than 1.5 nm) due to their instability under beam irradiation. However, we can easily assume that the number of Co and Pt atoms in a nanoparticle assembly stays constant during annealing, since material loss is prevented by the amorphous alumina layer. No Co or Pt atoms were detected between the particles. Therefore the excess of Co in the larger particles obviously comes from the smaller particles, which necessarily present an excess of Pt.

These experimental results demonstrate that growth mechanisms induce a size-dependent compositional change of CoPt NPs. Such an effect has already been observed in AuPd NPs [5,6], but up to now the origin of this key phenomenon for nanoalloy studies and applications has never been properly explained.

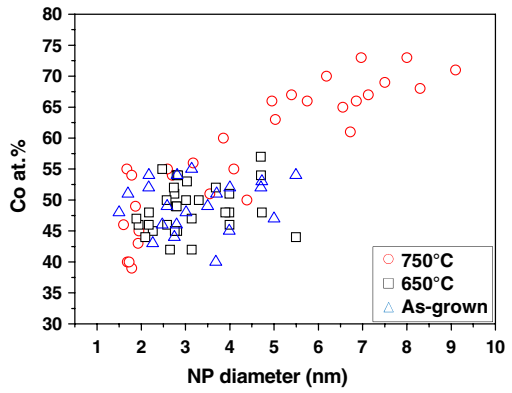

FIG. 2 (color online). Single particle composition measured by EDX nanoanalysis, as a function of their size. Blue triangle, as-grown NPs (sample *A*).; black square, NPs after 1 h at 650 °C (sample *B*); red circle, NPs after 1 h at 750 °C (sample *C*).

Cluster growth during annealing generally occurs through atom exchange between clusters, or through cluster diffusion and coalescence. If cluster diffusion and coalescence are the dominant processes, no variation of composition with size can occur. We can thus assume that at 750 °C (sample *C*), growth mainly occurs through Ostwald ripening: atoms evaporate from the clusters, diffuse onto the substrate, and condense on other clusters. However, these fluxes of atoms are driven by the difference in chemical potentials between large and small particles. These energetic factors cause small NPs to shrink because of their higher evaporation rate (i.e., higher chemical potential). Ostwald ripening is a thermally activated process, and two regimes can be distinguished: detachment limited kinetics and diffusion limited kinetics.

In order to understand the size-dependent concentration after annealing, we have observed the thermal behavior of monometallic NPs. Pure Pt and pure Co NPs were annealed during 1 h at 700 °C. Ostwald ripening is effective for both metals, but the cluster density after annealing is 3 orders of magnitude lower for Co than for Pt, indicating a much higher mobility of Co atoms. This higher mobility results either from a higher diffusion coefficient for Co than for Pt or a higher evaporation rate for Co atoms. An estimate of the rate of these different processes is given by the energy barriers. For evaporation to the substrate, the energy barrier ΔE is at least given by the energy difference between initial and final states. In a first approximation, neglecting cluster size effects, this leads to $\Delta E \geq E_a - E_c$, where E_a is the adsorption energy of an adatom on the surface and E_c is the bulk cohesive energy of the metal. E_c^{Co} and E_c^{Pt} are -4.386 and -5.853 eV, respectively [15]. The adsorption energy of Co and Pt atoms on graphene has been obtained by recent *ab initio* calculations [16,17]. They can be used as a first estimate of the adsorption energy of atoms on amorphous carbon ($E_a^{\mathrm{Co}} = -1.3$ eV and $E_a^{\mathrm{Pt}} = -1.2$ eV). The energy barrier for atomic evaporation from a large particle to the substrate is thus higher for Pt ($\Delta E^{\mathrm{Pt}} \geq 4.7$ eV) than for Co ($\Delta E^{\mathrm{Co}} \geq 3.1$ eV). These barriers are also much higher than the energy barriers for diffusion, especially on graphite where values as small as 0.1 eV are expected for metal atom diffusion [18]. In our case, atoms diffuse on amorphous carbon and the whole sample is covered by an alumina layer. However, the diffusion barrier should remain small as compared to the values of ΔE^{Co} and ΔE^{Pt}. Therefore, Ostwald ripening is first limited by the evaporation rate of atoms from the NPs. Moreover, from the Arrhenius dependence of the evaporation rate with the energy barrier ΔE^{Co} and ΔE^{Pt}, neglecting the contribution of the prefactors, one expects this rate to be about 10^8 times higher for Co than for Pt at 700 °C.

For Co_xPt_{1-x} alloys, these rates should be different since the cohesive energy is stronger due to the negative mixing enthalpy. Experiments have shown that the thermodynamic properties of Co_xPt_{1-x} alloys are well described by a regular solution model [19]. In that case, at equiatomic composition, the effect of the mixing on the evaporation rate should be the same for both species. Similarly to the case of pure metals, the evaporation rate from bimetallic NPs is thus much higher for Co atoms than for Pt atoms in the studied range of temperature. The decrease of NP density, i.e., the number of particles per unit area, is thus governed by the low evaporation rate of Pt atoms, whereas NPs' size and composition are governed by the fast exchange of Co atoms between the NPs. In that case, once equilibrium is achieved, the chemical potential of Co atoms is the same for each NP and for Co adatoms. The chemical potential for Co atoms is given by

$$\mu_{\mathrm{Co}} = \left.\frac{\partial G}{\partial N_{\mathrm{Co}}}\right|_{T,P}, \quad (1)$$

where N_{Co} is the number of Co atoms in the NP and G is the free enthalpy of the NP. $G = H - TS$, where $H = (N_{\mathrm{Co}} + N_{\mathrm{Pt}})h(x)$ and $S = (N_{\mathrm{Co}} + N_{\mathrm{Pt}})s(x)$ are the enthalpy and the entropy of Co_xPt_{1-x} particles, respectively. For Co_xPt_{1-x} bulk alloys, at zero pressure, the enthalpy per atom is written as

$$h(x) = xE_c^{\mathrm{Co}} + (1-x)E_c^{\mathrm{Pt}} + \Delta h_{\mathrm{mix}}, \quad (2)$$

where Δh_{mix} is the mixing enthalpy at this composition.

For entropy, an expression similar to Eq. (2) is obtained:

$$s(x) = xs^{\mathrm{Co}} + (1-x)s^{\mathrm{Pt}} + \Delta s_{\mathrm{mix}}, \quad (3)$$

with $s^{\mathrm{Co}} = 3.11 \times 10^{-4}\ \mathrm{eV \cdot K^{-1}\,at^{-1}}$, $s^{\mathrm{Pt}} = 4.32 \times 10^{-4}\ \mathrm{eV \cdot K^{-1}\,at^{-1}}$ [15], and

$$\Delta s_{\mathrm{mix}}(x) = -k[x\ln(x) + (1-x)\ln(1-x)] + \Delta s_{\mathrm{excess}}(x), \quad (4)$$

where Δh_{mix} and $\Delta s_{\mathrm{excess}}(x)$ have been measured for CoPt alloys in the 0.1–0.9 concentration range and in the 800 °C–1000 °C temperature range [19]. Extrapolating the data up to 750 °C, we obtain values of the mixing free enthalpy (Δg_{mix}) that can be quite well approximated by

$$\Delta g_{\mathrm{mix}}(x) = \Delta h_{\mathrm{mix}}(x) - T\Delta s_{\mathrm{mix}}(x) = \Delta g^0_{\mathrm{mix}} x(1-x), \quad (5)$$

with $\Delta g^0_{\mathrm{mix}} = -0.75$ eV/at.

For small NPs, the surface energy (E_s) is not negligible and then $G = H - TS + E_s$. Previous electron tomography studies have shown that CoPt NPs annealed at 750 °C are almost all spherical [14,20]. The surface energy can then be approximated by

$$E_s = \gamma(x)a_0^2(x)\pi(3N/2\pi)^{2/3}, \quad (6)$$

where a_0 is the lattice constant, γ is the mean surface free energy, and N is the total number of atoms in a NP. Since Pt and Co almost have the same surface free energy [21], the composition dependence of the surface free energy can be neglected. By neglecting the variation of a_0 with concentration, the chemical potential in a NP can be written as (Ref. [22])

$$\mu_{\mathrm{Co}}(T,x) = \mu^0_{\mathrm{Co}}(T) + \Delta g^0_{\mathrm{mix}}(1-x)^2 + \gamma a_0^2\left(\frac{2\pi}{3N}\right)^{1/3}, \quad (7)$$

where $\mu^0_{\mathrm{Co}}(T) = E_c^{\mathrm{Co}} - Ts^{\mathrm{Co}} = -4.704$ eV/at is the chemical potential for Co atoms in pure bulk cobalt.

For a given Co chemical potential, inverting Eq. (7) leads to a simple relation between composition and volume for the alloyed NPs:

$$x = 1 - \sqrt{\frac{\mu_{\mathrm{Co}}(T,x) - \mu^0_{\mathrm{Co}}(T) - \gamma a_0^2(2\pi/3N)^{1/3}}{\Delta g^0_{\mathrm{mix}}}}. \quad (8)$$

In a model of a sphere, particle diameter is easily obtained from N. The comparison between calculations using this analytical model and the size-dependent composition resulting from 1 h annealing at 750 °C (sample C) is presented in Fig. 3(a). Parameters have been determined using a least-squares fit. It shows that experimental data are well described by our simple model with $\Delta\mu_{\mathrm{Co}} = \mu_{\mathrm{Co}} - \mu^0_{\mathrm{Co}} = -0.021$ eV/at and $\gamma = 1.2\ \mathrm{J \cdot m^{-2}}$. Using experimental uncertainties both on NP diameter (± 0.3 nm) and composition (± 5%) we have calculated the errors on γ and μ_{Co} to be $0.1\ \mathrm{J \cdot m^{-2}}$ and 0.08 eV/at, respectively. This surface energy is small compared to recent density functional theory calculations at 0 K [23] [$1.7\ \mathrm{J \cdot m^{-2}}$ for (111) surfaces]. This discrepancy may have different origins. Firstly, the surface free energy is known to decrease with

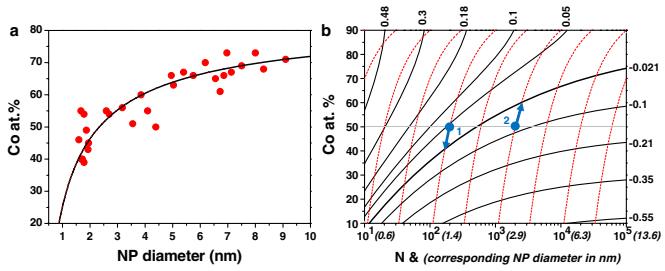

FIG. 3 (color online). (a) Co composition of single NPs as a function of their size after 1 h annealing at 750 °C. Comparison between experiments (red circle) and the theoretical curve (black line) obtained by using Eq. (8) with $\Delta\mu_{\mathrm{Co}} = -0.021$ eV/at and $\gamma = 1.2\ \mathrm{J \cdot m^{-2}}$. (b) Variation of the composition with the number of atoms per particle N (the corresponding NP diameter in nanometer is indicated). Plain black curves are obtained by using Eq. (8) with $\gamma = 1.2\ \mathrm{J \cdot m^{-2}}$ and a fixed $\Delta\mu_{\mathrm{Co}}$ indicated on the right and upper sides of the graph. Red dashed curves are obtained by using Eq. (9) for a fixed number of Pt atoms. The blue arrows show how the thermodynamic equilibrium of Co atoms (towards $\Delta\mu_{\mathrm{Co}} = -0.021$ eV/at, bold black line) induces the size-dependent compositional change of the particles labeled 1 and 2.

temperature. Secondly, atomic-structure ordering induces a higher mixing enthalpy, leading to a higher value for γ, and, most probably, the simple assumptions made about the shape evolution with size of the particles.

To provide a deeper understanding of growth mechanisms in nanoalloys, we have plotted in Fig. 3(b) the equipotentials corresponding to Eq. (8), for different μ_{Co} values, and the evolution of composition with size for particles where the number of Pt atoms (N^0_{Pt}) is constant. This assumption is valid in the limit of a much lower evaporation rate for Pt atoms than for Co atoms, and the composition inside a given NP follows the equation

$$x(N) = 1 - N^0_{Pt}/N. \quad (9)$$

As-grown NPs are in an out-of-equilibrium state: they are close to equiatomic composition [$x(N) = 0.5$], and consequently their Co chemical potential depends on their size. During annealing, $x(N)$ converges to the equipotential curve given by Eq. (8). Particles with a high μ_{Co} before annealing have a high evaporation rate so that their number of cobalt atoms decreases [particle 1 in Fig. 3(b)]. On the contrary, particles with a low μ_{Co} before annealing have a low evaporation rate so that their number of cobalt atoms increases [particle 2 in Fig. 3(b)]. After annealing, all the particles have the same μ_{Co} and this thermodynamic equilibrium induces a size-dependent composition. Note that this equilibrium is stable since desorption of Co atoms from a particle decreases its evaporation rate and vice versa. This stable equilibrium means that NPs' growth due to Co atoms' migration is suppressed. This situation is similar to the case of emulsions where droplets are stabilized by trapped species [24,25]. Experimentally, Ostwald ripening still occurs due to Pt evaporation, but on a much longer time scale, leading to a slow and continuous lowering of μ_{Co}.

In conclusion, we exploited the performances of EDX nanoanalyses to show the complex phenomena that arise during coarsening of nanoalloys. The size-dependent composition of CoPt NPs observed after annealing originates from the fact that the evaporation rate of atoms from particles is about a few orders of magnitude higher for Co than for Pt. Consequently, the system tends towards the thermodynamic equilibrium of Co atoms, and it is then impossible to maintain the initial composition of the particles. Therefore, this work illustrates the complexity of controlling together size and composition in nanoalloys, which is nevertheless crucial for understanding and exploiting their physical and chemical properties.

The authors acknowledge financial support from the ETNAA project (ANR-nano-018-04). We are grateful to Region Ile-de-France for convention SESAME 2000 E1435, for the support of the JEOL 2100F electron microscope installed at IMPMC (UMR7590).

*Corresponding author.
damien.alloyeau@univ-paris-diderot.fr

[1] I. M. Lifshitz and V. V. Slyozov, J. Phys. Chem. Solids **19**, 35 (1961).
[2] C. Wagner, Z. Elektrochem. **65**, 581 (1961).
[3] C. T. Campbell, Surf. Sci. Rep. **27**, 1 (1997).
[4] M. Kahlweit, Adv. Colloid Interface Sci. **5**, 1 (1975).
[5] M. Di Vece *et al.*, Phys. Rev. B **80**, 125420 (2009).
[6] A. A. Herzing *et al.*, Faraday Discuss. **138**, 337 (2008).
[7] D. Alloyeau *et al.*, Nanotechnology **18**, 375301 (2007).
[8] C. Langlois *et al.*, Faraday Discuss. **138**, 375 (2008).
[9] D. Alloyeau *et al.*, Ultramicroscopy **108**, 656 (2008).
[10] G. Cliff and G. W. Lorimer, J. Microsc. **1032**, 203 (1975).
[11] E. Van Cappellen, Microsc., Microanal., Microstruct. **1**, 1 (1990).
[12] C. E. Lyman, H. G. Stenger, Jr., and J. R. Michael, Ultramicroscopy **22**, 129 (1987).
[13] N. Braidy *et al.*, Microsc. Microanal. **14**, 166 (2008).
[14] D. Alloyeau *et al.*, Nature Mater. **8**, 940 (2009).
[15] D. R. Lide, *CRC Handbook of Chemistry and Physics* (CRC Press, Boca Raton, FL, 1998), 79th ed., pp. 5.13, 5.24.
[16] Y. Mao, J. Yuan, and J. Zhong, J. Phys. Condens. Matter **20**, 115209 (2008).
[17] C. K. Acharya, D. I. Sullivan, and C. H. Turner, J. Phys. Chem. C **112**, 13 607 (2008).
[18] P. Jensen, X. Blase, and P. Ordejón, Surf. Sci. **564**, 173 (2004).
[19] J. P. Cyr, J. Dellacherie, and D. Balesdent, J. Chem. Eng. Data **26**, 174 (1981).
[20] D. Alloyeau *et al.*, Ultramicroscopy **109**, 788 (2009).
[21] L. Vitos *et al.*, Surf. Sci. **411**, 186 (1998).
[22] See supplementary material at http://link.aps.org/supplemental/10.1103/PhysRevLett.105.255901 for the details of the calculation of Eq. (7).
[23] A. Dannenberg *et al.*, Phys. Rev. B **80**, 245438 (2009).
[24] A. S. Kabal'nov, A. V. Pertzov, and E. D. Shchukin, Colloids Surf. **24**, 19 (1987).
[25] A. J. Webster and M. E. Cates, Langmuir **14**, 2068 (1998).